Reaction Chemistry & Engineering

ROYAL SOCIETY OF CHEMISTRY

PAPER

View Article Online
View Journal | View Issue

Cite this: *React. Chem. Eng.*, 2024, **9**, 3211

Radio-frequency heating for catalytic propane dehydrogenation†

Ankush Rout,‡[a] Somtochukwu Lambert,‡[a] Aswin Nair,[a] Kailash Arole,[c] Debalina Sengupta,[b] Mark A. Barteau,[ad] Benjamin A. Wilhite*[a] and Micah J. Green*[ac]

Received 6th September 2024,
Accepted 10th September 2024

DOI: 10.1039/d4re00422a

rsc.li/reaction-engineering

In this paper, we have demonstrated radio frequency (RF) heating of susceptor nanomaterials coupled with conventional catalysts to enable a new class of heterogeneous catalytic reactors with localized, volumetric heating. The recent emphasis on industrial decarbonization has highlighted the need to reduce greenhouse gas emissions from chemical process heating. Existing industrial scale catalytic reactors use fuel-fired furnaces to achieve high temperatures which contributes to CO_2 emissions and requires on-site infrastructure. Compared to conventional heating, this work uses a power-to-chemicals route, where RF fields (1–200 MHz) are utilized to volumetrically heat RF-responsive carbon nanomaterials integrated with the catalyst. With the option of using renewable electricity sources, the greenhouse gas emissions associated with the process can be reduced, thereby contributing to industrial decarbonization. We demonstrate the use of an RF applicator to drive the highly endothermic propane dehydrogenation reaction on a Pt/alumina catalyst using carbon nanotubes as the RF susceptors. The propane conversion and propylene yield using RF heating were similar to those obtained when the reactor was heated externally in an oven (conventional heating (CH)) at 500 °C. After each reaction cycle, the catalyst was successfully regenerated by RF heating in air to remove deposited carbon.

Introduction

Catalytic reactions account for 80% of all chemical conversion processes,[1] with heating conventionally carried out by direct combustion of fossil fuel resources or indirect heating using steam,[2] resulting in significant greenhouse gas emissions and associated capital costs for utility infrastructure. External heating of fixed beds is prone to radial heat transport limitations, negatively affecting the utilization of catalyst and reaction selectivity.[3]

"Power-to-chemicals" represents an alternative approach where electrical energy (potentially from renewable or distributed energy sources) is used to drive chemical reactions.[4] By moving away from traditional combustion-based heating, a reduction in chemical plant footprint and greenhouse gas emissions may be achieved while enabling the utilization of renewable electrical resources. However, effective technologies for reactors that utilize electricity-to-heat have not yet achieved industrial scales.[5] Such technologies hold a key advantage of enabling rapid volumetric heating,[6] which avoids the radial temperature gradients of external heating, in principle improving temperature uniformity. Power-to-chemicals approaches have the potential to enable distributed (modular) manufacturing of chemicals from stranded resources.

Propylene is an important chemical used as a feedstock for the production of acrolein, polypropylene, acetone, acrylonitrile, and other industrial products.[7] Traditionally, propylene is obtained as a by-product of steam cracking process and fluid catalytic cracking (FCC) in which the main products are ethylene and gasoline respectively.[8] These technologies cannot keep up with the growing demand for propylene,[9] which calls for the gap to be filled by new on-purpose propylene technologies using feedstocks derived from shale gas. One such technology is propane dehydrogenation (PDH) and the production of propylene from PDH processes has doubled in the last decade.[10] Current commercial PDH processes include the Oleflex technology, which uses a Pt–Sn/Al_2O_3 catalyst, and the Catofin technology, which uses a Cr/Al_2O_3 catalyst.[11] In these

[a] *Artie McFerrin Department of Chemical Engineering, Texas A&M University, College Station, TX, 77843, USA. E-mail: benjaminwilhite@tamu.edu, micah.green@tamu.edu*
[b] *Energy Transition Institute, University of Houston, Houston, TX 77204, USA*
[c] *Department of Materials Science & Engineering, Texas A&M University, College Station, TX, 77843, USA*
[d] *Department of Chemistry, Texas A&M University, College Station, TX, 77843, USA*
† Electronic supplementary information (ESI) available. See DOI: https://doi.org/10.1039/d4re00422a
‡ Both authors contributed equally to this work.

processes, hydrogen is often added to the feed to reduce the formation of coke that deactivates the catalyst.[12] The PDH reaction is highly endothermic; thus, the process is energy intensive and requires high reaction temperatures (550–750 °C). These factors make PDH an excellent candidate for the power-to-chemicals approach.

Prior studies have reported electrical heating techniques to heat catalysts volumetrically. Wismann *et al.* reported the use of direct AC current applied to a FeCrAl-alloy tube with a nickel-impregnated washcoat to drive the steam methane reforming reaction to thermal equilibrium, thereby improving catalyst utilization and reducing byproduct formation.[13] Badakhsh *et al.* demonstrated the benefits of Joule heating of a NiCrAl catalyst to drive the ammonia decomposition reaction, resulting in lower reactor volume, higher efficiency, and higher power density compared to conventional reformers.[14] However, direct current heating (*i.e.*, Joule heating) of the catalyst may introduce safety issues, as it requires intimate electrical contact with both catalyst and reaction media.

Microwave (MW) fields (300 MHz–300 GHz) represent one means for indirect catalyst heating. Caiola *et al.* carried out studies of oxidative ethane dehydrogenation and reported similar ethane conversions by microwave heating at 450 °C compared to conventional heating (CH) at 650 °C.[15] Recently, Kwak *et al.* demonstrated the use of microwaves to carry out propane dehydrogenation on $PtSn/SiO_2$ catalyst pellets loaded in the channels of a SiC monolith; the monolith serves as a microwave susceptor. Their reaction experiments showed higher propylene formation rates using microwave heating compared to conventional heating without co-feeding hydrogen. The propylene selectivity was very high (>99.9%) with MW heating, and the amount of coke deposited was much less with MW heating than with CH. These authors hypothesized that coke precursors are MW susceptors, creating thermal hotspots that facilitate coke removal from active sites, reducing catalyst deactivation. The power required for heating with MWs was less than that for CH, suggesting that MWs are an efficient way of carrying out the PDH reaction.[16] However, the main drawback to microwaves is their limited penetration depth (d_p), which can result in temperature gradients across the catalyst.[17,18]

Radio-frequency (RF) fields (1–200 MHz) have shown rapid heating of electrically conductive nanomaterials like multi-walled carbon nanotubes,[19] single walled carbon nanotubes,[20] carbon fibers,[21] and SiC fibers.[22] The key benefit of using radio-frequency fields over microwaves is the greater penetration depth ($d_{p,RF}$ is approximately an order of magnitude higher than $d_{p,MW}$) because penetration depth is inversely proportional to frequency[23] ($d_p \propto 1/f$). Such fields are safe and versatile and can be delivered *via* various contact and non-contact applicators that are suitable for industrial scale up. The rapid heating of the susceptors materials noted above has allowed localized heating of thin films and composite materials for non-contact processing in electronics,[24] fiber processing,[25] and composite manufacturing.[26] Our group previously demonstrated a proof-of-concept use of RF fields to heat a hybrid susceptor/catalyst for endothermic reactions.[27] That work demonstrated that RF heating can drive methanol steam reforming over a conventional Pt/Al_2O_3 catalyst coupled with RF susceptors, achieving comparable conversion to oven-heated reactors. The present study targets PDH chemistry because of its industrial importance and the potential for utilization of stranded or distributed natural gas. RF heating of a PDH reactor at a large scale could have potential advantages. Commercial reactors for PDH are operated adiabatically, because heat adequate cannot be supplied by CH for the endothermic reaction. Volumetric heating with RF could, in principle, enable adiabatic operation, reducing reactor size and catalyst inventories by about 50%.

In this work, we demonstrate the thermal response of the monolith-support catalyst incorporating a RF susceptor and investigate the PDH reaction with RF *vs.* oven heating at 500 °C. We also compare the regeneration performance of the catalyst with RF heating and conventional oven heating at 340 °C. If RF-heated PDH can achieve competitive performance using only electricity, this technology can be a promising route for power-to-chemicals at industrial scale.

Material and methods

Materials

Functionalized multi-walled carbon nanotubes functionalized with –COOH groups (MWCNT-COOH) were purchased from Cheaptubes; Inductively Coupled Plasma-Mass Spectrometry (ICP-MS) analysis of MWCNT-COOH is shown in Table S1.† Alumina nano powder (13 nm) was purchased from Sigma Aldrich, and platinum on alumina (5 wt% on alumina, 44 μm) was purchased from Sigma Aldrich.

Catalyst sample preparation

Fig. 1 shows the schematic of the catalyst preparation. One-inch-long cordierite pieces were sectioned from a larger monolith with 2.85 mm square channels. The resulting sections contained 5 channels in a cross pattern. The catalyst-containing washcoat suspension was prepared using 5 wt% Pt/Al_2O_3, alumina nano powder, and functionalized multi-walled carbon nanotubes. These three components were mixed using tip sonication in an appropriate volume of deionized water, to produce a suspension of 6.5 wt% MWCNT-COOH, 3.1 wt% Pt, and 90.4 wt% alumina. The cordierite monolith sections were cleaned, and then dip coated in the washcoat suspension three times. An airbrush was used to clear the channels of excess solution followed by 30 minutes drying between washcoat applications. The coated cordierite pieces were dried in a fume hood for 24 hours at room temperature. As is typical when coating square channels, the thickness of the washcoat varied from 54 μm on the channel walls

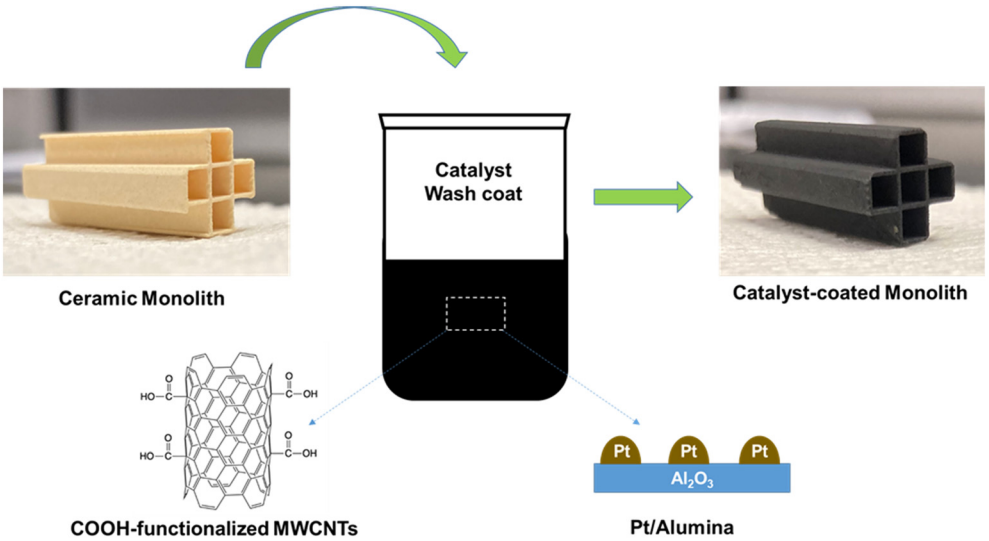

Fig. 1 Schematic of the preparation of the catalyst used for PDH reaction: ceramic monolith is dipped in the catalyst wash coat containing MWCNT-COOH, Pt, and alumina to obtain catalyst-coated monolith.

to 350 μm in the channel corners. Energy dispersive X-ray spectroscopy (EDS) mapping of the catalyst-coated monolith confirmed the presence of the components Al, O, Pt, and C (EDS and SEM results are shown in Fig. S1;† mapping at various regions showed a similar composition. The dried monolith catalysts were used for reaction tests after pre-treatment/activation in the reactor. Typical platinum loadings on the 1″ monolith sections following this procedure ranged from 2.0 to 4.0 mg, as determined from the total mass deposited and the Pt fraction in the washcoat suspension.

RF heating setup

The RF heating response of the washcoated monolith was tested under a "no-reaction" condition to determine optimal RF frequencies and power levels to achieve the temperatures required under reaction conditions. In the "no-reaction" experiments, a washcoated monolith was placed inside a 11 mm inner diameter quartz tube heated with an external parallel plate applicator mounted on a PEEK substrate. The spacing between the two copper plates of the applicator was 15 mm. The parallel plate applicator was supplied with RF power through a 50 ohm coaxial cable from a signal generator (Rigol Inc., DSG815) and a 100 W power amplifier (Mini-Circuits, ZHL-100W-GAN+). A FLIR infrared camera (FLIR Systems Inc., A500) was used to measure the maximum temperature of the catalyst by looking down the axis of the quartz tube. Note that the ends of the quartz tube remain open for temperature measurements with the FLIR.

The frequency that produces the maximum temperature rise can vary by a few MHz from experiment to experiment; thus, it was necessary to optimize the frequency for each experiment. For the frequency sweep test (heating rate *vs.* frequency), the catalyst was exposed to RF fields at 1 W for 1 s for varying frequencies in the range 1–200 MHz, followed by cooling for 13 seconds before moving to the next frequency. The dependence of the heating rate on frequency was calculated using the slope of the temperature ramp associated with each frequency, as illustrated in Fig. S6.†

To calibrate temperature measurement techniques applicable for reaction experiments, a far-focus pyrometer (Optris, OPTCTL3MHFF) was placed vertically above the horizontal quartz tube to measure the temperature of the catalyst along with FLIR camera aimed through the open end of the tube at the catalyst monolith to measure the maximum temperature.

Vector network analyzer (VNA)

VNA (SVA1015X, Siglent Technologies) was used to measure the S_{11} parameter for the bare parallel plate applicator, and the parallel plate applicator with catalyst.

Reactor setup

The reactor consisted of an 8 inch-long quartz tube with an inner diameter of 11 mm. The prepared monolith catalyst was placed inside the quartz tube with quartz wool placed around and at the ends of the monolith inside the reactor. The experimental setup consisted of four Alicat flow controllers (MFC) for hydrogen, propane, oxygen, and inert (argon or helium). Gases were fed to the reactor *via* these MFCs feed through a back-pressure regulator (0.5 atm). The system included a by-pass line for sampling the feed gas. The line from the reactor outlet was maintained at temperatures >80 °C with the aid of heating tapes. The product line was sampled continuously with a residual gas analyzer, RGA (Stanford Research Systems) through a capillary to decrease

the pressure to about 1 mbar at the inlet of the vacuum system of the RGA.

The reactor could be heated either externally using a conventional oven, or internally by absorption of RF radiation by the MWCNT-COOH in the catalyst washcoat. The RF source consisted of a signal generator and a power amplifier connected to the applicator through a 50 ohm coaxial cable. The applicator consisted of parallel copper plates mounted on opposite sides of the reactor tube. Temperature measurements in the case of RF heating were carried out using two close-focus pyrometers (Optris, A-OPTCTL3MH2CF3 and B-OPTCTL3H1CF3) focused on the monolith vertically above the horizontal quartz tube. The temperature measurements presented in the results section were generally recorded using the close-focus pyrometer B, although the close-focus pyrometer A provided important back-up when occasional data recording issues were encountered.

Experiments involving conventional heating were carried out in a Carbolite oven equipped with a temperature controller. A schematic of the reactor system is shown in Fig. 2. A metal thermocouple was inserted along the reactor axis into the central channel of the monolith to measure the temperature directly. To achieve the desired reaction temperature at steady state (500 °C), the oven setpoint was typically set about 2 °C above the desired temperature.

Reaction procedure

Monolith-supported catalysts were pretreated in the reactor prior to PDH experiments. The pre-treatment entailed reduction of the catalyst (60–120 mg) under 20% H_2/argon (75 mL min^{-1} total flowrate) at 500 °C for 30 minutes, after which the reactor was cooled to room temperature while purging with argon until the RGA detected no H_2. After argon purging, the reactor temperature was then ramped to the desired reaction temperature and the reaction feed mix (6% propane, C_3H_8/H_2 = 2) was introduced into the reactor. The products were continuously monitored with the residual gas analyzer (RGA). Gas/product analysis: the products of the reaction were analyzed with an on-line residual gas analyzer (RGA) furnished with a quadrupole mass spectrometer and Faraday cup detector. M/z ratios of 2 (for H_2) and 44 (for propane) were used for the direct determination of propane conversion from the feed and product stream signals and of hydrogen yield = (moles hydrogen formed/moles propane fed). The signal for m/z = 44 was used to determine the propane conversion and was scaled by the measured mass spectrometer cracking pattern to account for the contribution of propane to the signal for m/z = 29. Determination of the propylene yield required deconvolution of the signals for m/z = 41 and 29 common to both propane and propylene. The propane contribution was obtained by scaling the corrected propane signal for m/z = 29 by the ratio of the m/z = 41 and 29 signals in the measured cracking pattern for propane. The remainder of the m/z = 41 signal was assigned to propylene. Similarly, the observed signals with m/z ratios of 30 and 16 were also corrected for the propane contributions to obtain ethane and methane yields, respectively. The observed signal with m/z ratio of 27 was corrected for propane, propylene and ethane contributions to obtain

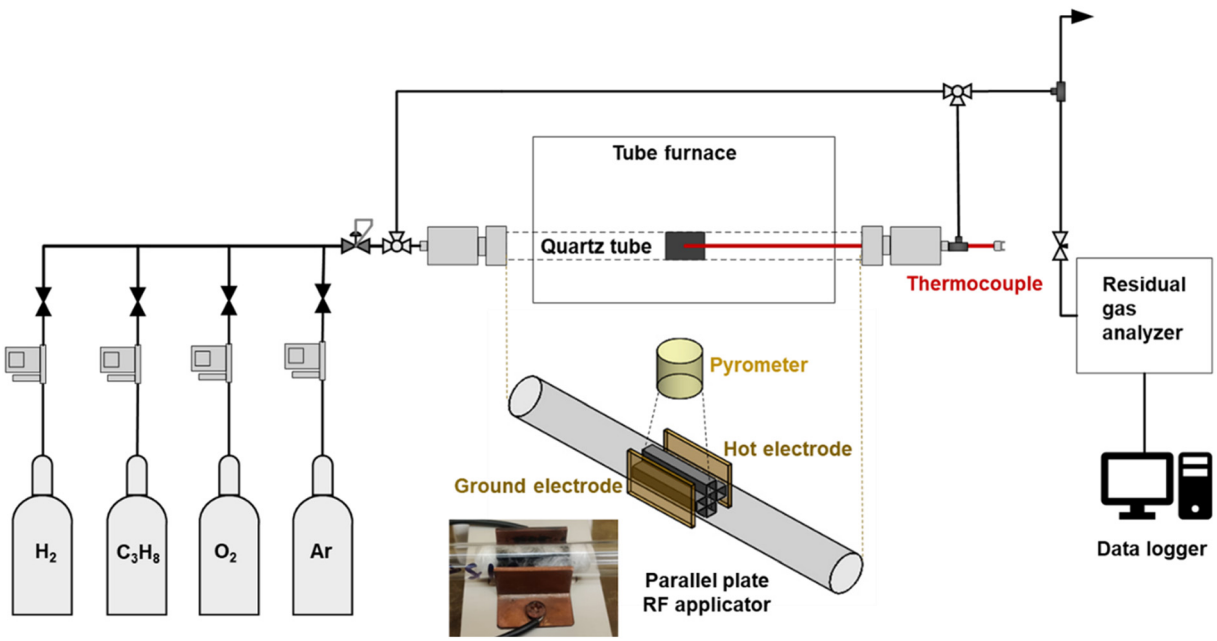

Fig. 2 Experimental setup for oven-heated and RF-heated propane dehydrogenation reaction (inset: parallel plate applicator setup for RF-heated PDH reaction, with photograph of the parallel plate applicator with the catalyst section of the reactor placed between the two parallel copper plates. The distance between the two parallel plates is 15 mm).

ethylene yield. The response factors used for hydrogen (m/z ratio of 2), and propane (m/z ratios of 44, and 29) were obtained by direct measurement of authentic samples of each, while the response factors for the detected products were calculated using their individually measured cracking pattern and equations presented in Ko *et al.*[28,29] The hydrogen content of the products determined using this approach was within 10% of the hydrogen supplied by the feed stream. The difference between the moles of carbon in the propane consumed and those contained in the gas phase reaction products propylene, ethane, ethylene, and methane, *i.e.*, the carbon missing from the overall mass balance, was attributed to carbon deposition on the catalyst. As shown below, this likely represents an overestimate of the extent of carbon deposition.

Regeneration procedure

After each reaction cycle, the reactor was flushed with argon until no H_2 was detected by the RGA, and the temperature was lowered to room temperature. During regeneration, 20% O_2/Ar (30 mL min^{-1}) gas flow was used at a temperature of 340 °C to burn off carbon deposits formed during the reaction. Product monitoring was continuous using the RGA.

Separate TGA experiments carried out in air demonstrated that the oxidation rate of the as-received MWCNT-COOH requires temperatures well above those used for catalyst regeneration in this study (340 °C) (Fig. S2†). In the TGA, the maximum rate of nanotube combustion was reached at 557 °C, and based on the kinetics of this process, at temperatures below 435 °C nanotube loss would be less than 1% for 1 h catalyst regeneration cycles. The absence of MWCNT-COOH combustion was confirmed by the absence of oxidation products in experiments in which a monolith washcoated with MWCNT-COOH, Pt/Al_2O_3, and nanopowder alumina was subjected to the regeneration conditions above in the reactor.

COMSOL simulation of parallel plate applicator

The simulations were performed in COMSOL Multiphysics v5.2 using the RF module. The geometry consisted of the two parallel copper plates, surrounding air and the lumped port. The input power was 30 W, and the frequency was 200 MHz. The electric field profile of the applicator was obtained after solving the electromagnetic field physics interface. The simulation parameters are listed in Table S2.†

Results and discussion

We first demonstrate the ability of the carbon nanotubes as RF susceptors to achieve the catalyst temperatures required to carry out the PDH reaction. We then describe how this system is incorporated into a full RF reactor with in-line product analysis and compare the performance of the RF reactor relative to conventional heating (CH).

RF susceptors and heating

Our formulation of the catalyst washcoat to be deposited on cordierite monoliths combined 5 wt% Pt in Al_2O_3, alumina nano powder, and functionalized multi-walled carbon nanotubes (MWCNT-COOH). To coat the monolith with this washcoat, an aqueous dispersion was prepared with these components. Since MWCNTs do not disperse in water due to the strong van der Waals interactions,[30] MWCNT-COOH were used as the RF susceptor. Heating of the conventional Pt/Al_2O_3 catalyst was carried out in parallel plate applicator at 3 W and it reached a meager 27 °C in 100 seconds, as compared to a MWCNT-COOH/Pt/alumina catalyst which reached 156 °C at 3 W in 100 seconds (as shown in Fig. S3†); this supports the usage of MWCNT-COOH as a RF susceptor and is vital for reaching very high reaction temperatures required for dehydrogenation reaction (~500 °C).

The ability of the parallel plate RF applicator (shown in Fig. 2) to heat the monolith catalyst is demonstrated in Fig. S4.† In these experiments, a continuous nitrogen gas purge was directed down the tube during RF heating to prevent oxidation of the carbon nanotubes at high temperatures. The FLIR camera was aimed down the open-ended quartz tube to directly record the temperature field across the face of the monolith during exposure. Our washcoated monoliths reached temperatures in excess of 500 °C at RF power levels of 25 W, demonstrating that this configuration is suitable for PDH reaction experiments. The thermal image of the cross section of the catalyst heated by RF shows the monolith heating from the inside out (Fig. S4c†). For subsequent experiments, a pyrometer was used to measure temperature through the tube sidewall (Fig. S5†) because thermal cameras cannot be used to measure the monolith temperature through the wall of the quartz tube. As described above, the frequency dependence of heating was also measured using pulsed RF exposure of the catalyst at a power of 1 W (a representative frequency sweep is shown in Fig. S6†). The temperature measurements for the frequency dependence tests were done using the FLIR camera. The S_{11} parameter was measured as a function of frequency (shown in Fig. S7†) for the parallel plate applicator with the catalyst and it was minimized at a frequency of 175 MHz with a value of −7.6 dB, which indicates only 17% of RF fields are reflected at that frequency, and this frequency corresponds to maximum absorption of RF absorption by the catalyst.

COMSOL simulations

The parallel plate applicator was modeled in COMSOL Multiphysics using the parameters in Table S1† to develop a better understanding of the electric field profile. Fig. S8a† shows the geometry of the applicator, which contains two parallel copper plates which are treated as perfect electric conductors in the simulation, and a lumped port.

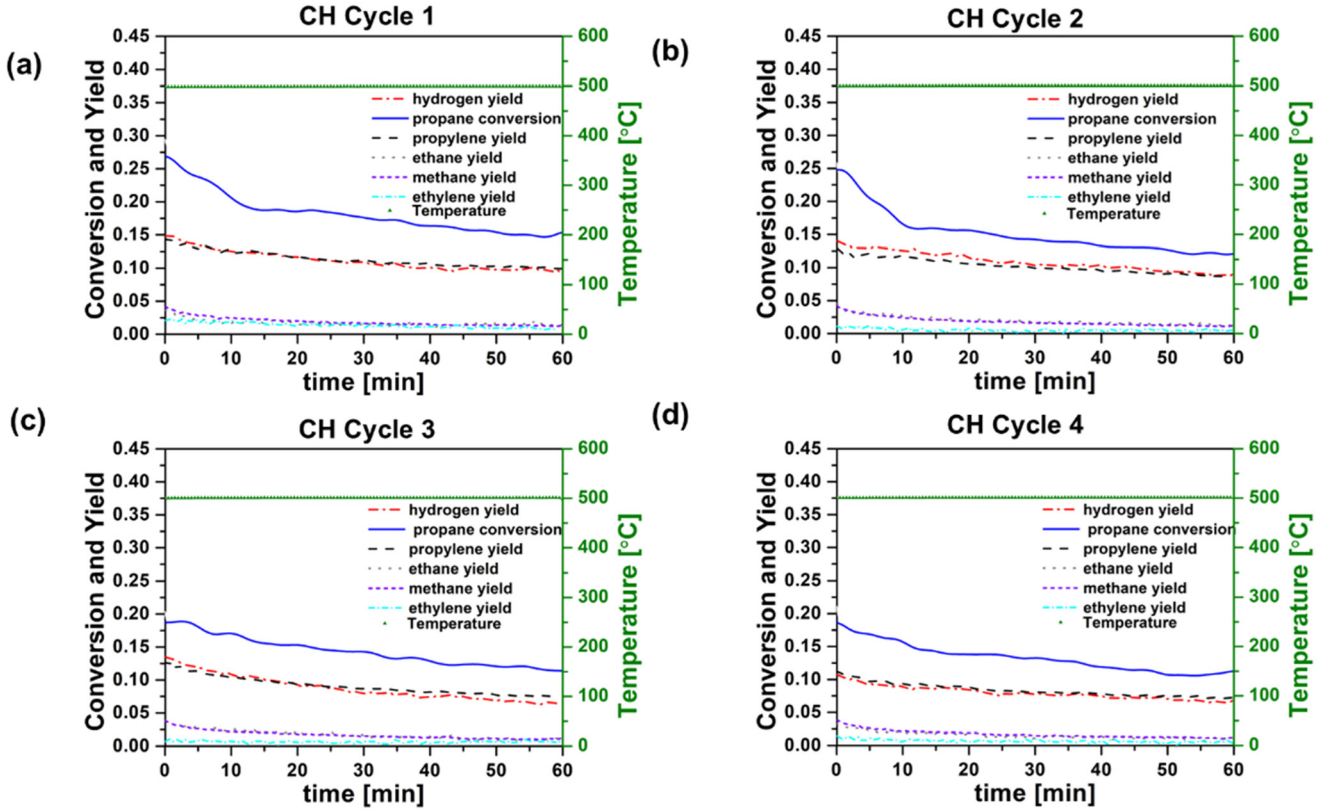

Fig. 3 Time-on-stream conversion and yield for propane dehydrogenation reaction in a washcoated monolith reactor during conventional (oven) heating (CH) for (a) cycle 1, (b) cycle 2, (c) cycle 3, and (d) cycle 4. Experimental conditions: 6% C_3H_8, 3% H_2, balance Ar, total flowrate = 75 sccm.

Fig. S8b† shows the distribution of the electric fields of the applicator at a frequency of 200 MHz and power of 30 W. The uniform electric field strength and the parallel streamlines between the two copper plates indicate the applicator is effective for volumetric RF heating of the hybrid catalyst/susceptor material.

Reactor performance

In order to provide a basis for evaluating RF heating of the catalyst, conventionally heated (CH) reaction–regeneration cycles were performed in an oven/tube furnace under similar experimental conditions. Co-feeding of H_2 was implemented because previous studies have indicated the potential to enhance PDH reaction coke resistance by reducing propylene adsorption strength or lowering coke precursor coverage.[12]

Fig. 3a–d and 4a–d show catalyst performance for 60 minute time-on-stream reactions on both fresh and regenerated catalysts, for conventional heating (CH) and radio frequency (RF) heating, respectively. Cycle 1 refers to the reaction on fresh catalysts, and cycles 2–4 refer to the reactions on regenerated catalysts. RF and CH catalytic reactions at 500 °C, 6% C_3H_8, H_2/C_3H_8 = 0.5, and low catalyst loading (64.3 mg and 61.0 mg for RF and CH, respectively) revealed comparable trends in the propane conversion and product yields over time for all four cycles. Calculated initial reaction rates ~0.045 mol propylene produced per mol_{Pt} s remained consistent across runs and align with those reported in the literature for Pt-based catalysts in PDH reactions.[31] Initial (at zero time on stream) propylene selectivity (mol propylene produced per mol propane converted) were *ca.* 50% due to competing reactions such as hydrogenolysis, deep dehydrogenation and coking[32] of the Pt/Al_2O_3 catalyst. These results are consistent with previous findings.[33] These side reactions indicated by the yields of methane and ethane, decreased significantly over the initial 10 minutes on stream for both fresh and regenerated catalysts under both CH and RF heating. In contrast, propylene yields were less affected by time on stream, and propylene selectivity reached *ca.* 60 to 80% after 60 minutes in all cases. Propylene selectivity was marginally higher in CH reaction cycles compared to RF reaction cycles, while propane conversion rates were higher in RF reaction cycles. Using the same pre-treatment and reaction conditions, blank experiments were performed with the empty reactor tube, an uncoated cordierite monolith, and a monolith coated with MWCNT-COOH and alumina to confirm the absence of gas phase chemistry at 500 °C. In all cases the yield of light (C1 and C2) hydrocarbons was an order of magnitude less than that observed under catalytic reaction conditions. The power requirement for each RF

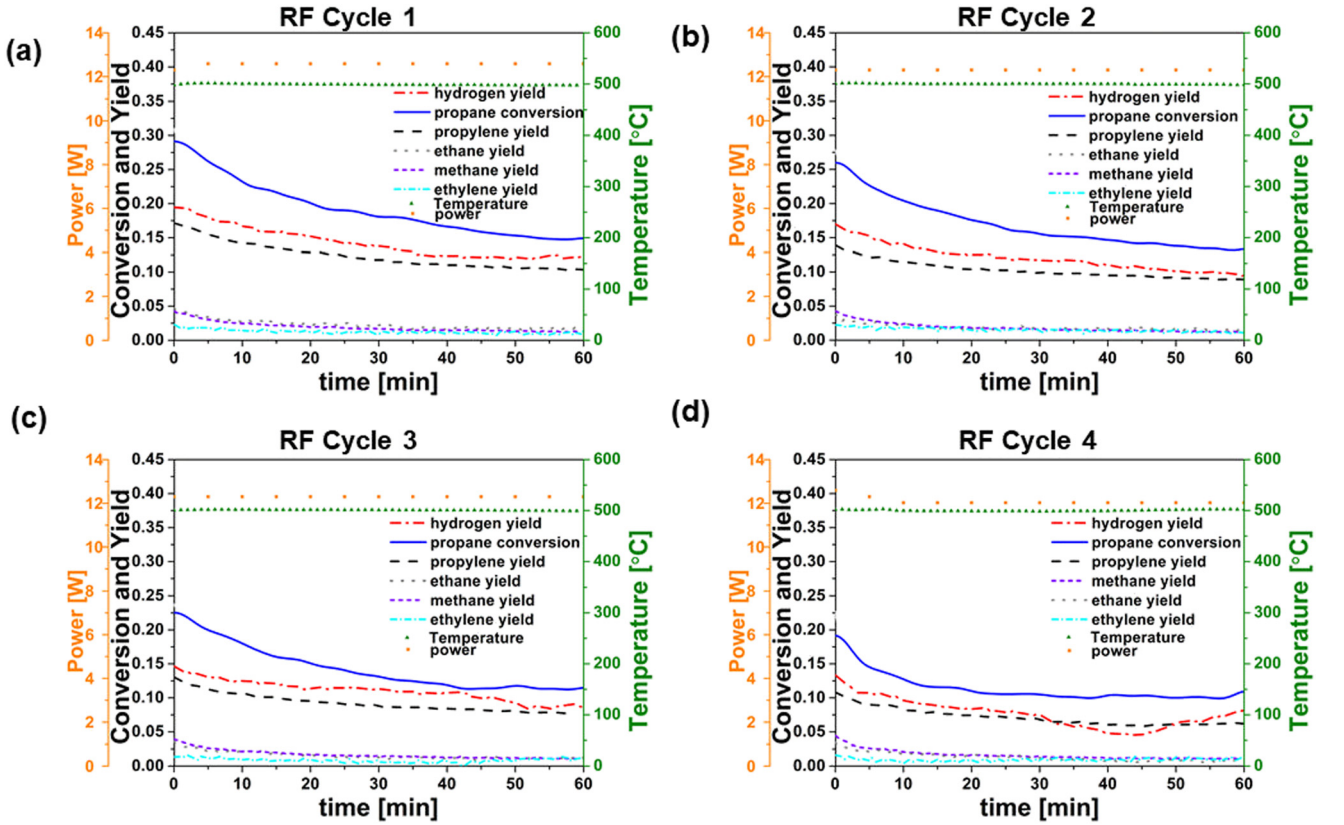

Fig. 4 Time-on-stream conversion and yield for propane dehydrogenation reaction in a washcoated monolith reactor during RF heating for (a) cycle 1, (b) cycle 2, (c) cycle 3, and (d) cycle 4. The radio frequency during each reaction cycle was chosen to be 166 MHz. Experimental conditions: 6% C_3H_8, 3% H_2, balance Ar, total flowrate = 75 sccm.

reaction cycle did not vary significantly, indicating that the performance of MWCNT-COOH as susceptors was unaffected by reaction and regeneration cycles.

The conversion of propane to form methane (CH_4), ethane (C_2H_6), ethylene (C_2H_4), and coke represent undesirable side reactions.[34] Cracking of propane to methane and ethylene, as well as the formation of coke precursors, can occur both by gas phase free radical reactions and by catalytic reactions on Pt. The rapid decrease in methane and ethane production with time on stream suggests that the dominant pathway in these experiments is *via* surface reactions, as gas phase reactions should not be affected by changes in catalyst activity. Hydrogenolysis of C–C bonds on Pt catalysts is well known to compete with hydrogenation and dehydrogenations reactions. Bimetallic catalysts are typically employed in processes such as PDH and catalytic reforming of gasoline-range hydrocarbons in order to suppress hydrogenolysis, which is a structure-sensitive reaction (*i.e.*, it depends on the availability of multi-atom Pt ensembles).[31,35] For our unpromoted Pt catalysts, coke deposition on the catalyst likely disrupts the Pt ensemble sites required for hydrogenolysis. In both RF and CH reaction cycles, the decrease with time in the production of methane and ethane relative to propylene suggests that hydrogenolysis is likely the predominant pathway leading to methane and ethane. Overlapping yields of methane and ethane species in both the RF and CH reaction cycles support this hypothesis. The key point, however, is that the reaction processes for formation of C_1–C_3 hydrocarbons are not sensitive to the method of energy supply, whether CH or RF, in our experiments. RF heating does not appear to promote gas phase chemistry, alter catalytic chemistry, or change catalyst properties relative to CH heating. If RF heating promoted gas phase reactions, one would expect that these would persist as the catalyst deactivated with time on stream. The similarity of the conversion and selectivity results after the initial ~10 minutes on stream (when coke deposition and propane cracking to methane and ethane are observed) for both RF and CH experiments suggests that this is not the case.

Catalyst regeneration

After each reaction cycle on our unpromoted Pt/Al_2O_3 catalyst, regeneration is essential to remove accumulated coke deposits. Coke deposits can form on the active metal particles *via* side reactions such as deep dehydrogenation and polymerization of reaction intermediates.[36] The catalyst regeneration process, conducted at 340 °C with a

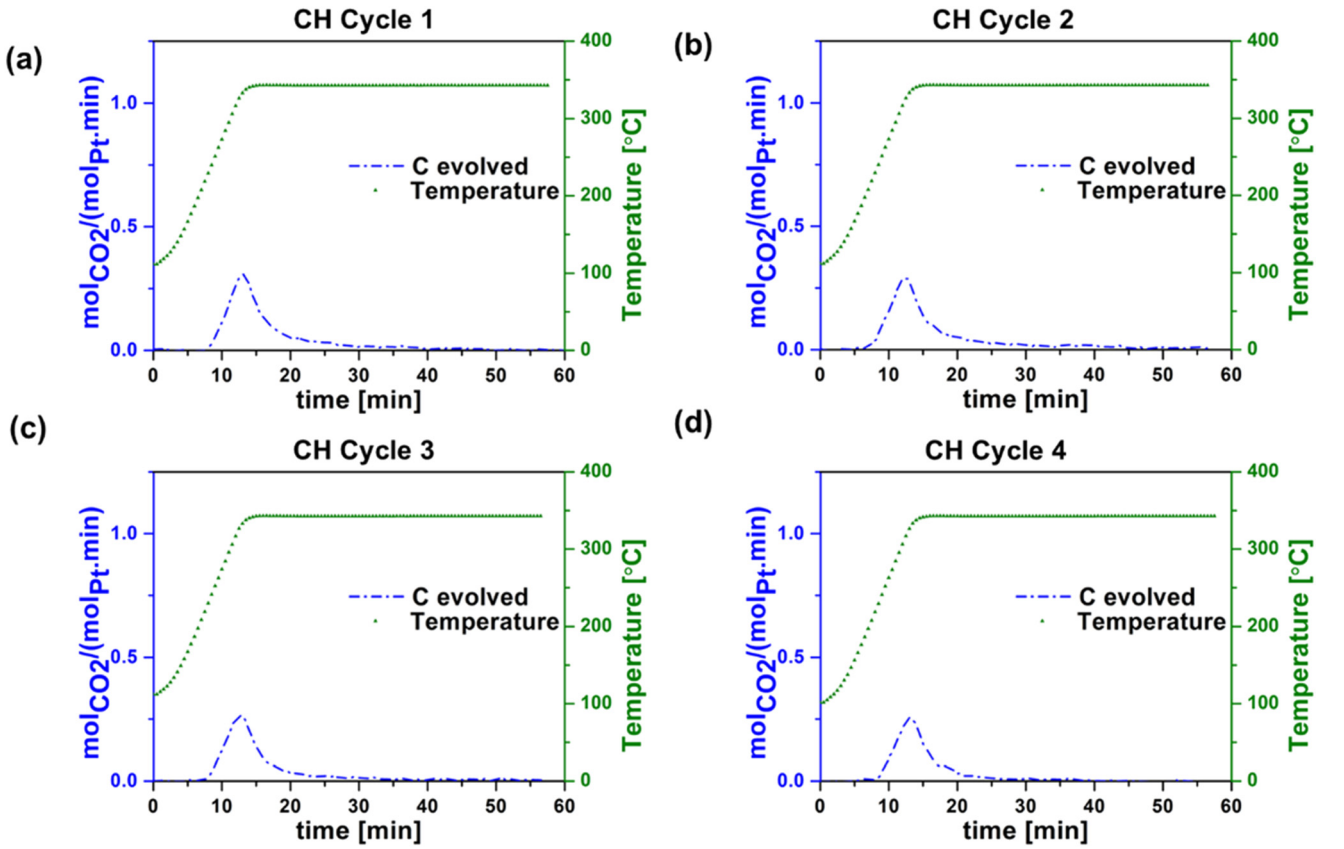

Fig. 5 Carbon evolved during regeneration step during conventional (oven) heating (CH) in (a) cycle 1, (b) cycle 2, (c) cycle 3, and (d) cycle 4. Experimental conditions: 30 sccm (20 O_2 in argon).

20% O_2/Ar flow of 30 mL min^{-1}, facilitates the burn-off of coke, resulting in the production of CO_2. The temperature for regeneration cycles was chosen to avoid burning of the carbon nanotubes, which has been shown to occur above 435 °C.[37] Fig. 5a–d and 6a–d present catalyst regeneration (coke-burning) data after each reaction cycle shown in Fig. 3 and 4, for conventional heating (CH) and radio frequency (RF) heating, respectively. The experiments we carried out after each reaction in the CH and RF-heated setups consist of four cycles. In Fig. 5 and 6, cycle 1 refers to the catalyst regeneration that followed the first reaction cycle, and cycles 2, 3 and 4 to the catalyst regeneration steps that followed the second, third, and fourth reaction cycles, respectively. One aspect in which there is an apparent difference between CH and RF heating is in the amount of carbon (coke) burn-off during regeneration. The difference between the moles of carbon in the propane consumed and those contained in the gas phase reaction products propylene, ethane, ethylene, and methane was attributed to coke deposition during propane dehydrogenation while the carbon evolved as CO_2 during regeneration resulted from the burn-off of coke during regeneration. SEM images of the RF heated post-reaction catalyst (shown in Fig. S9†) reveal no major morphological difference from the SEM images of the pre-reaction catalyst (Fig. S1†).

Table 1 summarizes the propane conversion, propylene selectivity, and coke formation results corresponding to the data in Fig. 3–6. The amount of coke deposited in RF-heated reaction cycles appeared to be comparable to that deposited during CH reaction cycles based on the mass balance closure with respect to volatile products in each case. CO_2 yield during oxidative regeneration of the catalyst at 340 °C and 30 mL min^{-1} 20% O_2/Ar exhibited higher CO_2 peaks in RF regeneration cycles 1–4 compared to CH regeneration cycles 1–4, indicative of the efficiency of RF regeneration compared to the CH regeneration at these conditions.

The cause of the observed increase in coke burn-off in the case of RF heating is unclear. Given that coke burn-off rates increase with temperature, one possibility is the existence of localized hot spots at the micrometer or smaller scale. The SEM indicates that the washcoat is porous and non-homogeneous at the micron scale (Fig. S1†), such that isolated CNT networks could potentially create small local hot spots with increased coke burn-off.

Conclusions

In this work, we demonstrate the effective utilization of COOH-functionalized multi-walled carbon nanotubes as RF susceptor to achieve the necessary temperature for the propane dehydrogenation (PDH) reaction. This system was

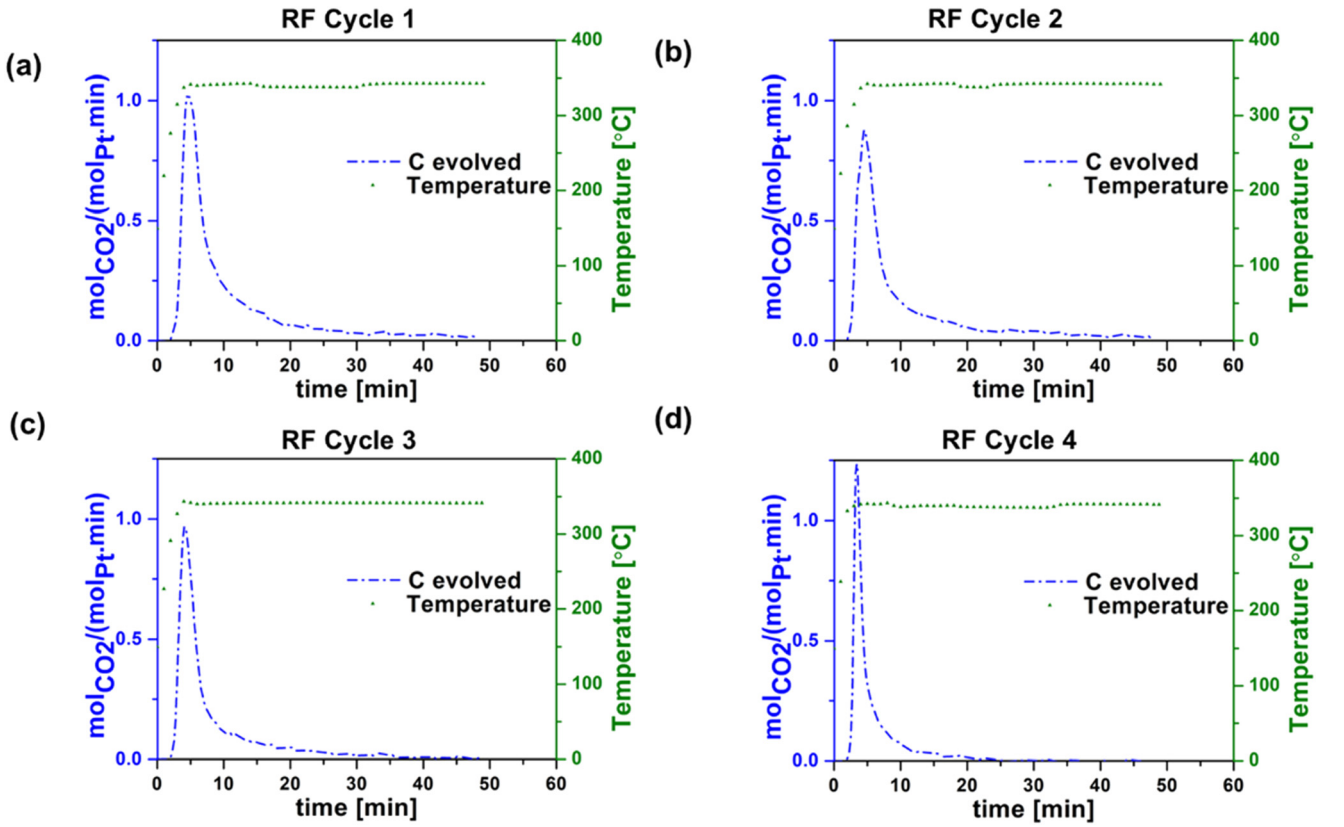

Fig. 6 Carbon evolved during regeneration step during RF heating in (a) cycle 1, (b) cycle 2, (c) cycle 3, and (d) cycle 4. Experimental conditions: 30 sccm (20% O_2 in argon).

Table 1 Summary of results for Pt/Al_2O_3 catalyst heated using parallel plate RF applicator and conventional oven (CH)

	RF				CH			
	Cycle 1	Cycle 2	Cycle 3	Cycle 4	Cycle 1	Cycle 2	Cycle 3	Cycle 4
Initial conversion, [%]	31	28	24	23	29	26	20	21
Final conversion, [%]	14	13	11	10	15	12	11	10
Initial C_3H_6 yield [%]	17	14	13	11	14	13	13	11
Final C_3H_6 yield [%]	10	9	8	6	10	9	8	7
Initial C_3H_6 selectivity [%]	55	50	55	48	49	50	62	53
Final C_3H_6 selectivity [%]	73	69	69	63	68	76	67	72
Coke deposited [mol mol_{Pt}^{-1}]	46.3	44.5	35.3	26.8	52.1	32.2	38.9	36.0
Coke burned [mol mol_{Pt}^{-1}]	6.2	5.2	4.3	2.9	2.3	2.4	1.9	1.6
Ratio of coke burned to coke deposited	0.13	0.12	0.12	0.11	0.04	0.07	0.05	0.05
Initial propylene productivity [$mol_{C_3H_6}$ mol_{Pt}^{-1} s^{-1}]	0.056	0.046	0.043	0.036	0.048	0.045	0.045	0.038

successfully integrated into an RF reactor with in-line product analysis, allowing for direct comparison with the conventional heating (CH) method. The formulation of the catalyst washcoat, comprising 5 wt% Pt in Al_2O_3, alumina nano powder, and MWCNT-COOH deposited on cordierite monolith, facilitated volumetric RF heating of the hybrid catalyst/susceptor material. Thermal imaging confirmed the efficacy of the parallel plate RF applicator for achieving volumetric heating across the monolith catalyst at observable length scales. A comparison of catalyst performance between RF and CH heating revealed similar trends in propane conversion and product yields over time. However, RF heating did not alter reaction performance, but did lead to somewhat greater carbon burn-off in the regeneration experiments. Catalyst regeneration was demonstrated for both RF and CH heating by burning the coke deposited on the Pt/Al_2O_3 catalyst. The application of RF-driven catalytic reactions offers a promising avenue for alternative heating methods in the chemical industry. Challenges remain, however, both in the delivery of electromagnetic radiation inside metal reactors, and in measuring catalyst temperatures under these conditions.

Data availability

Supporting data for this work are provided in the ESI.† Additional data is available upon request.

Conflicts of interest

The authors declare no conflict of interest.

Note added after first publication

This article replaces the version published on the 19th of September 2024. The RSC acknowledges that an error was made on first publication and the value in the last paragraph of the introduction has now been corrected from 400 °C to 340 °C.

Acknowledgements

The authors would like to acknowledge the use of TAMU Microscopy & Imaging Center (RRID: SCR_022128) for the use of SEM and EDS equipment. The authors would like to acknowledge the help of Ramu Banavath for carrying out the ICP-MS measurements. The authors would like to thank Nik Suphavilai and Fatima Mahnaz for carrying out the TGA experiments. The authors would also like to acknowledge Dr. Bruce Hook (Dow, retired), Dr. Dan Hickman (Dow), Tanya Snook (Keller ISD), Shawn Hull (Midland Christian School), and James Cooper Allen (TAMU) for their inputs and discussion. This work was funded by US National Science Foundation (Grant CMMI-2228861).

References

1 Z. Ma and F. Zaera, Heterogeneous Catalysis by Metals, in *Encyclopedia of Inorganic and Bioinorganic Chemistry [Internet]*, ed. R. A. Scott, Wiley, 2nd edn, 2005, available from: **https://onlinelibrary.wiley.com/doi/10.1002/9781119951438.eibc0079**.

2 J. K. Kim, Studies on the conceptual design of energy recovery and utility systems for electrified chemical processes, *Renewable Sustainable Energy Rev.*, 2022, **167**, 112718.

3 M. Bowker, J R H Ross (ed): Heterogeneous Catalysis: Fundamentals and Applications, *Catal. Lett.*, 2012, **142**(11), 1411.

4 D. Schack, L. Rihko-Struckmann and K. Sundmacher, Structure optimization of power-to-chemicals (P2C) networks by linear programming for the economic utilization of renewable surplus energy, in *Computer Aided Chemical Engineering [Internet]*, ed. Z. Kravanja and M. Bogataj, Elsevier, 2016, pp. 1551–1556, (26 European Symposium on Computer Aided Process Engineering, vol. 38), available from: **https://www.sciencedirect.com/science/article/pii/B9780444634283502630**.

5 L. Zheng, M. Ambrosetti and E. Tronconi, Joule-Heated Catalytic Reactors toward Decarbonization and Process Intensification: A Review, *ACS Eng. Au*, 2024, **4**(1), 4–21.

6 E. Meloni, E. Saraceno, M. Martino, A. Corrado, G. Iervolino and V. Palma, SiC-based structured catalysts for a high-efficiency electrified dry reforming of methane, *Renewable Energy*, 2023, **211**, 336–346.

7 S. Chen, X. Chang, G. Sun, T. Zhang, Y. Xu and Y. Wang, *et al.*, Propane dehydrogenation: catalyst development, new chemistry, and emerging technologies, *Chem. Soc. Rev.*, 2021, **50**(5), 3315–3354.

8 A. Agarwal, D. Sengupta and M. El-Halwagi, Sustainable Process Design Approach for On-Purpose Propylene Production and Intensification, *ACS Sustainable Chem. Eng.*, 2018, **6**(2), 2407–2421.

9 Z. P. Hu, D. Yang, Z. Wang and Z. Y. Yuan, State-of-the-art catalysts for direct dehydrogenation of propane to propylene, *Chin. J. Catal.*, 2019, **40**(9), 1233–1254.

10 M. Monai, M. Gambino, S. Wannakao and B. M. Weckhuysen, Propane to olefins tandem catalysis: a selective route towards light olefins production, *Chem. Soc. Rev.*, 2021, **50**(20), 11503–11529.

11 Y. Dai, J. Gu, S. Tian, Y. Wu, J. Chen and F. Li, *et al.*, γ-Al2O3 sheet-stabilized isolate Co2+ for catalytic propane dehydrogenation, *J. Catal.*, 2020, **381**, 482–492.

12 S. Saerens, M. K. Sabbe, V. V. Galvita, E. A. Redekop, M. F. Reyniers and G. B. Marin, The Positive Role of Hydrogen on the Dehydrogenation of Propane on Pt(111), *ACS Catal.*, 2017, **7**(11), 7495–7508.

13 S. T. Wismann, J. S. Engbæk, S. B. Vendelbo, F. B. Bendixen, W. L. Eriksen and K. Aasberg-Petersen, *et al.*, Electrified methane reforming: A compact approach to greener industrial hydrogen production, *Science*, 2019, **364**(6442), 756–759.

14 A. Badakhsh, Y. Kwak, Y. J. Lee, H. Jeong, Y. Kim and H. Sohn, *et al.*, A compact catalytic foam reactor for decomposition of ammonia by the Joule-heating mechanism, *Chem. Eng. J.*, 2021, **426**, 130802.

15 A. Caiola, B. Robinson, S. Brown, X. Wang, Y. Wang and J. Hu, Oxidative ethane dehydrogenation under thermal vs. microwave heating over Ga/ZSM-5 and GaPt/ZSM-5, *Catal. Commun.*, 2023, **176**, 106631.

16 Y. Kwak, C. Wang, C. A. Kavale, K. Yu, E. Selvam and R. Mallada, *et al.*, Microwave-assisted, performance-advantaged electrification of propane dehydrogenation, *Sci. Adv.*, 2023, **9**(37), eadi8219.

17 I. de Dios García, A. Stankiewicz and H. Nigar, Syngas production via microwave-assisted dry reforming of methane, *Catal. Today*, 2021, **362**, 72–80.

18 A. I. Stankiewicz and H. Nigar, Beyond electrolysis: old challenges and new concepts of electricity-driven chemical reactors, *React. Chem. Eng.*, 2020, **5**(6), 1005–1016.

19 C. B. Sweeney, A. G. Moran, J. T. Gruener, A. M. Strasser, M. J. Pospisil and M. A. Saed, *et al.*, Radio Frequency Heating of Carbon Nanotube Composite Materials, *ACS Appl. Mater. Interfaces*, 2018, **10**(32), 27252–27259.

20 M. Anas, Y. Zhao, M. A. Saed, K. J. Ziegler and M. J. Green, Radio frequency heating of metallic and semiconducting single-walled carbon nanotubes, *Nanoscale*, 2019, **11**(19), 9617–9625.

21 S. S. Dasari, A. Sarmah, R. D. Mee, A. N. Khalfaoui and M. J. Green, Joule Heating of Carbon Fibers and Their

Composites in Radio-Frequency Fields, *Adv. Eng. Mater.*, 2023, **25**(10), 2201631.

22 N. Patil, X. Zhao, N. K. Mishra, M. A. Saed, M. Radovic and M. J. Green, Rapid Heating of Silicon Carbide Fibers under Radio Frequency Fields and Application in Curing Preceramic Polymer Composites, *ACS Appl. Mater. Interfaces*, 2019, **11**(49), 46132–46139.

23 M. Gao, J. Tang, J. A. Johnson and S. Wang, Dielectric properties of ground almond shells in the development of radio frequency and microwave pasteurization, *J. Food Eng.*, 2012, **112**(4), 282–287.

24 V. K. Hicks, M. Anas, E. B. Porter and M. J. Green, High-throughput screening of printed carbon nanotube circuits using radio frequency heating, *Carbon*, 2019, **152**, 444–450.

25 N. Patil, A. C. Camacho, N. K. Mishra, P. Singhla, C. B. Sweeney and M. A. Saed, *et al.*, Radio Frequency and Microwave Heating of Preceramic Polymer Nanocomposites with Applications in Mold-Free Processing, *Adv. Eng. Mater.*, 2019, **21**(8), 1900276.

26 D. Debnath, X. Zhao, M. Anas, D. L. Kulhanek, J. H. Oh and M. J. Green, Radio frequency heating and reduction of Graphene Oxide and Graphene Oxide - Polyvinyl Alcohol Composites, *Carbon*, 2020, **169**, 475–481.

27 N. Patil, N. K. Mishra, M. A. Saed, M. J. Green and B. A. Wilhite, Radio Frequency Driven Heating of Catalytic Reactors for Portable Green Chemistry, *Adv. Sustainable Syst.*, 2020, **4**(11), 2000095.

28 E. I. Ko, J. B. Benziger and R. J. Madix, Reactions of methanol on W(100) and W(100)-(5 × 1)C surfaces, *J. Catal.*, 1980, **62**(2), 264–274.

29 V. S. Lusvardi, M. A. Barteau and W. E. Farneth, The Effects of Bulk Titania Crystal Structure on the Adsorption and Reaction of Aliphatic Alcohols, *J. Catal.*, 1995, **153**(1), 41–53.

30 J. Dai, R. M. F. Fernandes, O. Regev, E. F. Marques and I. Furó, Dispersing Carbon Nanotubes in Water with Amphiphiles: Dispersant Adsorption, Kinetics, and Bundle Size Distribution as Defining Factors, *J. Phys. Chem. C*, 2018, **122**(42), 24386–24393.

31 J. J. H. B. Sattler, J. Ruiz-Martinez, E. Santillan-Jimenez and B. M. Weckhuysen, Catalytic Dehydrogenation of Light Alkanes on Metals and Metal Oxides, *Chem. Rev.*, 2014, **114**(20), 10613–10653.

32 A. H. Motagamwala, R. Almallahi, J. Wortman, V. O. Igenegbai and S. Linic, Stable and selective catalysts for propane dehydrogenation operating at thermodynamic limit, *Science*, 2021, **373**(6551), 217–222.

33 H. N. Pham, J. J. H. B. Sattler, B. M. Weckhuysen and A. K. Datye, Role of Sn in the Regeneration of Pt/γ-Al2O3 Light Alkane Dehydrogenation Catalysts, *ACS Catal.*, 2016, **6**(4), 2257–2264.

34 F. Yang, J. Zhang, Z. Shi, J. Chen, G. Wang and J. He, *et al.*, Advanced design and development of catalysts in propane dehydrogenation, *Nanoscale*, 2022, **14**(28), 9963–9988.

35 I. Lezcano-González, P. Cong, E. Campbell, M. Panchal, M. Agote-Arán and V. Celorrio, *et al.*, Structure-Activity Relationships in Highly Active Platinum-Tin MFI-type Zeolite Catalysts for Propane Dehydrogenation, *ChemCatChem*, 2022, **14**(7), e202101828.

36 B. Feng, Y. C. Wei, W. Y. Song and C. M. Xu, A review on the structure-performance relationship of the catalysts during propane dehydrogenation reaction, *Pet. Sci.*, 2022, **19**(2), 819–838.

37 Z. Zhao, Z. Yang, Y. Hu, J. Li and X. Fan, Multiple functionalization of multi-walled carbon nanotubes with carboxyl and amino groups, *Appl. Surf. Sci.*, 2013, **276**, 476–481.